

promoting access to White Rose research papers



Universities of Leeds, Sheffield and York
<http://eprints.whiterose.ac.uk/>

This is the published version of an article in the **Journal of Geophysical Research D: Atmospheres, 117 (20)**

White Rose Research Online URL for this paper:

<http://eprints.whiterose.ac.uk/id/eprint/76600>

Published article:

Schepanski, K, Wright, TJ and Knippertz, P (2012) *Evidence for flash floods over deserts from loss of coherence in InSAR imagery*. Journal of Geophysical Research D: Atmospheres, 117 (20). ARTN D20101. ISSN 0148-0227

<http://dx.doi.org/10.1029/2012JD017580>

Evidence for flash floods over deserts from loss of coherence in InSAR imagery

K. Schepanski,¹ T. J. Wright,¹ and P. Knippertz¹

Received 6 February 2012; revised 12 September 2012; accepted 13 September 2012; published 16 October 2012.

[1] Flash floods in complex terrain play an important role for sediment transport in arid regions and thus potentially for dust production, but observations of these phenomena are scarce over most of the world's deserts. Here, methods from radar interferometry, applied to 8 years (2003–2010) of ENVISAT Advanced Synthetic Aperture Radar data over the northwestern Sahara, are used to demonstrate the potential of these data to identify significant flash floods. Loss of coherence between two consecutive images is indicative of changes in surface characteristics. Tropical Rainfall Measuring Mission daily precipitation estimates, together with the digital elevation model from the Shuttle Radar Topography Mission, are analyzed to assess the likelihood of these changes to be related to flash floods. Four interferometric pairs representing periods with different rainfall amounts are examined with regard to changes in surface characteristics caused by precipitation. To do this, ratios of coherences are calculated, highlighting the changes in soil texture through loss of coherence in particular for desert valleys. Many pixels within wadis show large coherence during dry periods and a significant loss during wet periods, while others show low coherence irrespective of rainfall, possibly due to Aeolian processes. In the long term, findings from this study will be used to investigate the relation between flash floods and interannual variability of local dust emission fluxes.

Citation: Schepanski, K., T. J. Wright, and P. Knippertz (2012), Evidence for flash floods over deserts from loss of coherence in InSAR imagery, *J. Geophys. Res.*, 117, D20101, doi:10.1029/2012JD017580.

1. Introduction

[2] Flash floods are a frequent and important phenomenon in semi-arid and arid regions. Besides their ability to destroy roads and buildings, flash floods are important for the local hydrology as they replenish aquifers and groundwater reservoirs [e.g., Morin *et al.*, 2009]. Flash floods also impact on geomorphology as they change the particle size distribution of the topsoil due to the generation of fresh deposits, but also the shape and the level of the channel bed, as well as vegetation [e.g., Friedman *et al.*, 1996, and references therein]. Over arid regions, flash floods preferentially occur in the vicinity of mountains, where orography triggers the development of deep moist convection ultimately able to cause intense rainfall. The role of flash floods for supplying fine sediments for dust production is currently debated.

[3] Recent studies using satellite observations show that numerous dust sources are located in the foothills of the Saharan mountains, i.e. the Hoggar Massif, the Air, the Adra des Iforas, the Tibesti, and the Ennedi in the central Sahara, the Red Sea Mountains in the eastern Sahara, and the Atlas

Mountains and the Akhdra Massif at the northern boundary of the Sahara [Schepanski *et al.*, 2007, 2009, 2012]. Over these areas, dust emission follows a pronounced diurnal cycle with dust sources being most active during the morning hours between 0600 and 0900 UTC, when the nocturnal low-level jet (LLJ) breaks down and wind speed at the surface suddenly increase [Schepanski *et al.*, 2009].

[4] Generally, dust emission is controlled by sediment supply and wind speeds [e.g., Bagnold, 1941; Marticorena and Bergametti, 1995; Shao, 2001; Crouvi *et al.*, 2012]. Thus, dust emission can be inhibited by either lack of high wind speeds or by surface characteristics like vegetation cover, soil texture, and soil moisture.

[5] Studies on the frequency of dust source activation show a marked interannual variability [Schepanski *et al.*, 2009, 2012], the reasons of which are not fully understood. Possible explanations include changes in local supply of sediments suitable for dust emission, in soil moisture, or in meteorological conditions. The former can be expected to be important for dust sources in complex terrain, where drainage systems and dry valleys form the landscape [e.g., Reheis and Kihl, 1995; Shao, 2008]. The bottoms of these desert valleys are typically covered by a mixture of fine- and coarse-fraction sediments like silt, sands, and rock debris. Most of these sediments are pluvial; generated during wet periods, when heavy rainfall produces strong runoff accumulating at lower levels, which can lead to flash floods. Depending on the slope of the drainage system, its catchment area, and the accumulated rainfall,

¹School of Earth and Environment, University of Leeds, Leeds, UK.

Corresponding author: K. Schepanski, School of Earth and Environment, University of Leeds, Leeds LS2 9TJ, UK. (k.schepanski@leeds.ac.uk)

the water masses can carry lots of sediments and rock debris washed off from the barren soil surface within a short period of time. Within the flow, new soil particles are generated by collision and abrasion. However, where the flow slows down, particles settle due to gravitation and form a fresh layer of pluvial sediments. This process depends on buoyancy, and therefore on particle size. Fine particles are likely to settle where the slope and ultimately the flow velocity decrease. These pluvial sediments are of interest for dust emission, as they consist of a mixture of different particle size classes, a prerequisite to mobilize soil particles, but also to uplift and mix them into the boundary layer [e.g., *Bagnold*, 1941; *Gillette et al.*, 1980; *Reheis and Kihl*, 1995; *Kok and Renno*, 2009]. Locations with a “fresh” layer of sediments suitable for uplift are more prone to dust emission than those that are lacking certain particle size classes due to previous dust emission events. In the latter case, higher wind velocities are required for dust uplift [*Gillette et al.*, 1982].

[6] *Reheis and Kihl* [1995] evaluate dust emission from alluvial and playa dust sources in southern Nevada and California by analyzing dust deposition rates from a sampler network. Data were collected at 55 sites during a 5-year period (1984–1989). Meteorological observations were obtained from 32 stations distributed over the research domain. Analysis of local deposition rates together with rainfall measurements suggests different response patterns in local dust fluxes to rain events. Increased dust fluxes are observed over two different source types: alluvial sources and playa sources. Dust fluxes were increased at stations located in alluvial source regions during the year with increased rainfall rates or the following year. Fresh debris flows and recently flooded low ground characterize the surface. Such disturbed soil is very prone to Aeolian erosion after a relatively short response time. Increased dust fluxes were observed at stations located near playas during the year following high rainfall rates. *Reheis and Kihl* [1995] also observed that recently dried out playa floors are very prone to wind erosion as the flooding reduces stabilizing vegetation. Runoff flooding the playa deposits sediments that can be easily deflated. As the playa floor is not as well drained as the alluvial sediments, the response time is longer. A detailed investigation of dust emission from dry and wet playas is discussed by *Reynolds et al.* [2007] for the Mojave Desert, USA.

[7] Here, we present results of a study on the identification of fluvial soil erosion after intense rainfall events. The study is designed as a feasibility study and is the first step in investigating the relevance of the atmospheric water cycle, in particular rainfall, for the generation of fine, alluvial sediments, and thus ultimately on the interannual variability of dust emission fluxes from these sources. In the following, we will focus on the impact of intensive rainfall events causing flash flooding for sediment transport. We analyze the relation between these events and changes in surface structure using methods from space-borne radar interferometry. Space-borne radar data have been used previously to obtain information on surface characteristics. *Marticoarena et al.* [2006] relate Synthetic Aperture Radar (SAR)/ERS C-band radar data to radar backscatter coefficients in order to retrieve aerodynamic roughness lengths over arid and semi-arid regions. Interferometric Synthetic Aperture Radar (InSAR) data have also been used to identify and monitor sediment erosion/deposition, slope motion, river inundation, and land

subsidence [*Smith*, 2002, and references therein]. The aim of this study is to better understand the usefulness of InSAR data in combination with rainfall estimates to detect flash floods and associated sediment transports in dust source regions. To the best of our knowledge, such an approach has not been tested before.

[8] Results from this feasibility study will help to identify areas of recent fluvial erosion and will form the basis for more systematic studies on interannual dust source variability.

2. Study Area

[9] The area of interest for this study is located at 27.5–28.5°N and 10.5–9.5°W (Figure 1). Strong convective rainfall events can occur year-round, but are most frequently related to upper-level troughs over the adjacent Atlantic Ocean during winter (November–April). Studies analyzing satellite images highlight this area as a dust source area [*Schepanski et al.*, 2007]. Ground observations have suggested the general relevance of alluvial deposits in desert valleys for dust emission [e.g., *Reheis and Kihl*, 1995]. Hence, the combination of occasional intensive rainfall events and the presence of alluvial sediments suggest that dust emitted from this area is likely to originate at least partly from the fine size fraction of sediments covering the bottom of the valley floors.

[10] The complexity and heterogeneity of the terrain, which determines surface runoff and soil erosion can be described by metrics such as elevation, ruggedness, and flow accumulation. The flow accumulation depends on the size of the catchment area and represents the capacity of individual drainage systems. Here, the logarithm of the flow accumulation is used to identify individual drainage systems (Figure 1). In addition to the elevation, ruggedness represents the heterogeneity of the surface and thus the spatial variability of the topography.

[11] The study area comprises some elevated terrain south of the Draâ Valley in southern Morocco (Figures 1a and 1b). The highest elevations are found in the center of the domain with decreasing terrain toward its borders (Figure 1b). Topographic gradients are steepest in the north, where distinctive slopes are found. Steep valleys open toward low ground, where alluvial fans and temporally flooded plains covered by alluvial sediments are common features of the surroundings. The elevation decreases more gently toward the east and south. The ruggedness of the surface is higher in the northern and western part of the area (Figure 1c), where the desert valleys are steeper. In the southeastern part of the area, the drainage systems are flatter and the topography is less rugged.

3. Data and Method

[12] Images from space-borne SARs provide detailed information (spatial resolution of a few 10s of meters) on ground topography, surface structures, and surface features. If these properties remain relatively constant between consecutive SAR acquisitions, and if the density of vegetation is low, an interferogram can be constructed, in which the phase content is temporally coherent [e.g., *Massonnet and Feigl*, 1998; *Burgmann et al.*, 2000]. Changes in local surface structure cause random phase shifts at individual pixels in interferograms that are not spatially coherent. Thus, consecutive images for the same location with similar viewing geometries are suitable to retrieve changes in surface structure [e.g., *Lee*

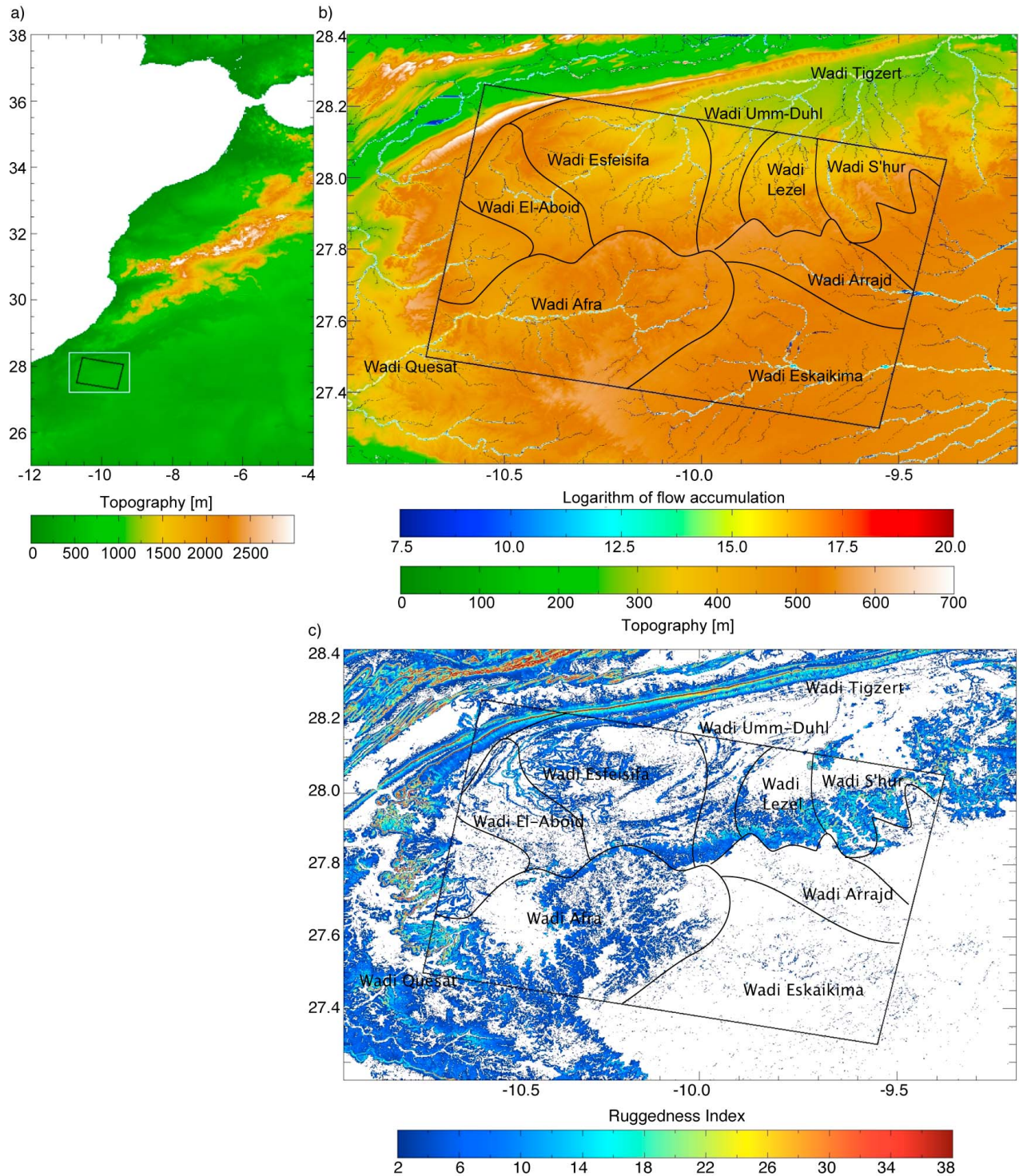


Figure 1. Geographical overview. (a) Map of the area of interest in northwestern Africa. (b) Zoom into the white box in Figure 1a. (c) Ruggedness index calculated from SRTM DEM following *Riley et al.* [1999] using TopoToolbox [*Schwanghart and Kuhn*, 2010]. The black box surrounds the area covered by track 409 for the chosen InSAR images in all three panels. Topography is represented by green-brownish/white shades in Figures 1a and 1b; flow accumulation representing the importance of individual drainage systems for water run-off is given in rainbow colors (blue-yellow-red) in Figure 1b. Higher flow accumulations are associated with stronger sediment movements. Individual catchment areas are separated by black contours in Figures 1b and 1c.

and Liu, 2001; Fielding et al., 2005]. Invariant surface characteristics lead to temporally coherent phase. Changes in surface characteristics are incoherent in time, which can be measured by spatial decorrelation.

[13] The coherence γ of an interferogram i has multiple contributions γ_i such as viewing geometry $\gamma_{i,geo}$, vegetation cover $\gamma_{i,veg}$, and surface structure $\gamma_{i,change}$, as summarized in Equation 1:

$$\gamma_i = \gamma_{i,geo} \cdot \gamma_{i,veg} \cdot \gamma_{i,change} \quad (1)$$

Although flying on the same orbit, the position of the satellite shifts slightly and thus the viewing geometry does not stay the same. The difference in position is expressed by the baseline, providing a measure for the vertical and horizontal shift in the position of the satellite between two acquisition times. Small baselines indicate close positions.

[14] The shift in satellite position between two acquisitions, expressed by the perpendicular baseline, changes the viewing angle, which ultimately leads to phase changes. The coherent backscatter phase becomes increasingly different in a random way, which results in decorrelation (baseline decorrelation). Knowledge on the exact position of the satellite and the topography can reduce this effect, but usually a small contribution to the interferogram remains. Thus, the topographic contribution to the interferogram is a function of the perpendicular baseline. An overview on recent advances in InSAR is given by Hooper et al. [2012].

[15] Information on surface topography are retrieved from travel time of back-scattered radar beams providing that the exact position of the satellite is known. For flat terrain, longer travel times are related to longer distances. For steep terrain, received radar signals may be superimposed, depending on slope incident angle relative to the radar beam incident angle. The travel time is reduced for positions at higher terrain, and thus the calculated distance is closer and may overlay with other positions. This effect, named foreshortening or layover, leads to a reduced data accuracy. Due to the incident angle of 23° of the radar beam, foreshortening and layover are likely to occur over the study area, in particular over the northern part.

[16] The ENVISAT ASAR instrument operates at the microwave C-band (wavelength 5.6 cm). Thus, clouds do not affect the measurements. Under ideal conditions such use in laboratories, the radar beam penetration depth for alluvial soil is estimated to be 0.1–0.2 m [see Schaber and Breed, 1999, Table 1]. Therefore we assume that the SAR data represent the surface structure. Flooded or by moisture saturated surfaces change the back-scatter characteristics of the soil, but as evaporation rates are high over the desert and alluvial sediments are well drained, flooding over the study area can be assumed to disappear during hours to a couple of days after the precipitation event.

[17] For radar interferometry the perpendicular component of the baseline is a crucial parameter. The main effect of large perpendicular baselines is the changing viewing angle, which means ground obstacles like buildings but also rock formations and mountains are observed under a slightly different geometry. In addition, multiple reflections within dense vegetation canopies before the radar beam is finally scattered back to the receiver can cause significant decorrelation over short time intervals. This effect is called volume scattering.

The phase of the return signal from the volume is highly sensitive to the incidence angle, and hence incoherence due to volume scattering is a function of the geometry of the acquisition. Change in vegetation also alters the reflected radar beam. Depending on the vegetation type, vegetation growth and decay can also occur on timescales shorter than an orbit repeat (here 35 days) and lead to loss of coherence between the two radar images.

[18] In addition, the coherence between two images is affected by soil surface processes. In contrast to the viewing geometry and vegetation cover, soil surface changes can be caused by natural or anthropogenic processes. Construction works and agricultural activity (e.g. ploughing) are prominent examples for anthropogenic changes in soil surface structure. Natural processes changing soil surface conditions are, for example, volcanic eruptions, landslides, earthquakes, or flooding. In this study we focus on changes in surface structure related to fluvial activities caused by flash floods.

[19] To create a link between identified surface changes and rainfall events, four consecutive steps are taken:

[20] 1. ENVISAT SAR IS2 images (product level 0, VV polarization mode (Vertical polarization transmitted/Vertical polarization received), swath width 100 km) for orbit track 409 (overpass every 35 days) over northwest Africa (Figure 1) are used to calculate interferograms for consecutive images using the Caltech/Jet Propulsion Laboratory (JPL) ROI_PAC (Repeat Orbit Interferometry PACage) software [Rosen et al., 2004]. The following non-standard processing procedure is applied: After image co-registration and baseline calculation, the interferogram is computed at 1 range look and 5 azimuth looks (ca. 20 m × 20 m resolution) and initially flattened by removing the phase contribution due to the satellite orbit and the curved Earth. We then correct for the topography's contribution to the phase using the DEM (Digital Elevation Model) retrieved from the SRTM as reference topography, interpolated to a horizontal grid resolution of 30 m. In the next step, the spatial correlation is calculated, using a running, triangular weighted window of 3 × 3 pixels (60 m × 60 m). The correlation is an estimate of the interferometric coherence and provides information on changes between the two overpasses. To keep effects from factors other than rainfall to a minimum, consecutive images (separated by 35 days) are chosen. To reduce the uncertainty of the interferogram due to viewing geometric aspects, the perpendicular baseline (differences of the instrument's position) of the chosen pairs needs to be at a minimum [Ahmed et al., 2011].

[21] 2. In the second step, rainfall events with a significant strength and thus potential to cause changes in surface structure due to runoff and sediment wash-out are identified. Here, daily rain rate estimates from the TRMM (Tropical Rainfall Measuring Mission [Huffman et al., 2007]) 3B42 (version 6) product are analyzed. The estimates are provided on a grid with 0.25° horizontal spacing. The typically short but intense rainfall over arid and semi-arid land tends to be underestimated by TRMM retrievals by up to 15–30% [Chiu et al., 2006]. However, as no rain gauge measurements are available for the study region, the TRMM rainfall product provides the best available estimate.

[22] 3. External impacts on surface structure changes besides those caused by rainfall need to be excluded as well as possible. The area is practically uninhabited, no dirt roads cross the region, such that impacts from anthropogenic

activities are most likely negligible. Although most parts of the area are characterized by barren soil, limited vegetation may grow from time to time. To investigate vegetation growth as a reason for loss of coherence between two radar images, the Aqua MODIS (Moderate Resolution Imaging Spectroradiometer) 16-day NDVI (Normalized Difference Vegetation Index) product MYD.Q13 (version 5, horizontal resolution: 250 m) is used. The accuracy of NDVI vegetation estimates may be limited through several factors such as surface inhomogeneity, atmospheric variations, sensor calibration, and instrument drift, which lead to increased uncertainties in particular for low NDVI values. Additionally, the spectral signature of vegetation, which depends on growing phase and photosynthetic activity, the spectral signature of barren soil surface fraction, and the solar geometry contribute to uncertainty in NDVI values and may lead to misinterpretation of temporal changes in vegetation [Okin, 2007]. Nevertheless, several studies have demonstrated the applicability of NDVI to monitor vegetation in arid and semi-arid environments [e.g., Weiss *et al.*, 2004; Schmidt and Karnieli, 2000; Fensholt *et al.*, 2009]. The region of interest shows some seasonal vegetation growth, but no significant vegetation cover is found for the time covered by the interferometric pairs discussed here. Vegetation growth in arid and semi-arid regions is found by Schmidt and Karnieli [2000] to respond to rainfall with a time lag of 1–2 month, depending on phenotype. Thus, decorrelation due to vegetation growth is more likely to be found for 70-day repeats than for the here analyzed 35-day repeat overpass.

[23] 4. In step four, we calculate coherence ratios to highlight areas of decorrelation. Although areas of loss of coherence already stand out in the interferograms, this method allows us to highlight differences between two interferograms covering different time periods. Two interferograms, the first covering a dry period (no rainfall between the two images) and the second covering a wet period (significant rainfall recorded between the two overpasses) are set in ratio. Stationary decorrelations, e.g. due to viewing geometry or topographic effects are removed from the ratio images and only differences in decorrelation caused by other factors stand out [Lee and Liu, 2001]. Here, a relation to rainfall can be assumed as the loss of coherence for the dry period interferogram represents a typical degree of decorrelation. Locally, the contribution of Aeolian processes to decorrelation may also be significant. The coherence ratio method can only be applied to interferometric pairs with small baseline differences, as otherwise the impact of the viewing geometry on the interferogram cannot be assumed to be similar.

[24] In Section 4 the coherence for five (four + reference) different interferograms is discussed. Each 35-day period covered by the interferogram is characterized by different amounts of precipitation.

4. Results

[25] Figure 2 shows the coherence of the interferograms for the five 35-day pairs 20031223-20040127 (referred to as i1), 20040824-20040928 (referred to as i2), 20041102-20041207 (referred to as i3), 20100420-20100525 (referred to as i4), and 20100803-20100907 (referred to as i5) (dates are in the format of *yyyymmdd*, *yyyy* = year, *mm* = month, and *dd* = day; for more information see Table 1). Coherent phases are depicted

by bright shading (values close to 1), areas with loss of coherence have dark shading (values close to 0). According to TRMM no precipitation occurred during i1 (Table 1), which can therefore serve as an estimate of a typical background loss of coherence for a 35-day period and will be used as a reference interferogram. Coherence values are well above 0.8 over large parts of the study area, particularly in the southeast of the domain (Figure 2a), with a spatial mean of 0.68. Greatest losses of coherence are found to the north of the main watershed, particularly in the upstream catchment areas of wadis Umm-Duhl, Lezel, and S'hur (see Figure 1 for locations) and to a smaller extent in the western parts of the domain. These are most likely due to foreshortening or layover effects along steep topography and rugged terrain caused by superimposed back-scattered radar signals. The other notable feature is the loss of coherence in the Wadi Afra area in the southwest that reflects the fluvial structures seen in Figure 1. These might be caused by foreshortening due e.g. to larger rocks along the wadi bed or isolated trees or shrubs. Similar but weaker effects are found for the wadis Eskaikima, Arrajd, and Esfeisifa.

[26] The corresponding interferogram for 20040824-20040928 (i2) shows an overall higher degree of decorrelation (Figure 2b) with a spatial mean of 0.63. Differences between i1 and i2 can be separated from background decorrelation (e.g., due to different viewing geometry) by calculating the ratio between the two interferograms as shown in Figure 3a. If this ratio is 1, the two interferograms have identical coherence. Values larger than 2 show a significant loss of coherence in i2 relative to the background level represented by i1.

[27] The largest values of the coherence ratios are found in the steeper terrain in the northeast of the domain in parts of the catchment areas of the wadis Lezel and S'hur. In terms of fluvial structures parts of the wadis Afra and Arrajd as well as the upper part of Wadi S'hur stand out. Also the alluvial fan and floodplain region (triangle-like feature) where the wadi enters the low lands is represented by a strong loss of coherence. Aeolian processes, i.e. erosion and deposition, are very likely contribution to the decorrelation there. The relation of the coherence between the two interferograms can also be displayed in the form of scatterplots for individual pixels (Figure 4a). The decorrelation between i1 and i2 is evident from the large scatter around the diagonal (marked in blue) with a clear tendency to populate the red-shaded bottom right corner (i.e. larger loss in coherence in i2 than i1), leading to a flat linear regression line with a gradient of 0.6 (marked in red). According to TRMM widespread precipitation fell during this period with an area-averaged accumulation of 15 mm (Table 1). 91 % of this precipitation fell within the 48 hours beginning the day after the first image of the interferometric pair with a spatial maximum (32 mm) in the southwestern corner of the domain (Figure 5a). As the water absorption ability of the soil is expected to be poor due to present aridity, a large fraction of the water probably ran off and eroded the barren soil surface [Esteves and Lapetite, 2003]. This supports the assumption that both the fluvial and also some of the more patchy patterns seen in Figure 2b could be the direct consequence of the action of rainwater on the soil, such as channel erosion and sheetwash (hillslope erosion) [e.g., Fanning, 1999; Hughes *et al.*, 2009].

[28] The interferogram i3 (Figure 2c) shows a decorrelation distribution similar to i1. The ratio of i1 to i3 displayed in

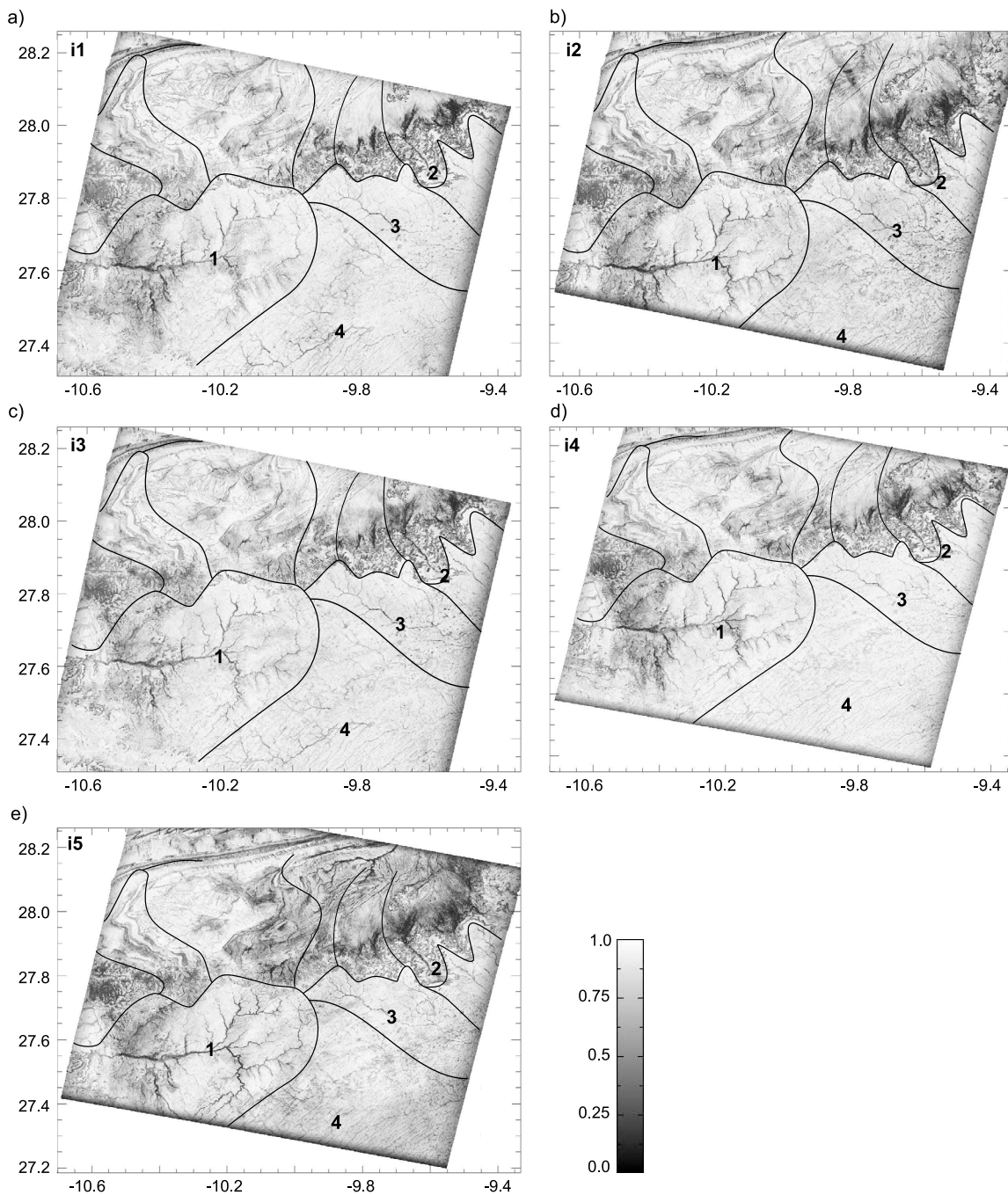


Figure 2. Interferograms showing the coherence for five different pairs of ENVISAR ASAR radar images covering a 35-day period: (a) 2003-12-23 and 2004-01-27 (referred to as i1), (b) 2004-08-24 and 2004-09-28 (referred to as i2), (c) 2004-11-02 and 2004-12-07 (referred to as i3), (d) 2010-04-20 and 2010-05-25 (referred to as i4), and (e) 2010-08-03 and 2010-09-07 (referred to as i5). Numbers refer to geographical names given in the text: 1 - Wadi Afra, 2 - region of Wadi Umm-Duhl, Wadi S'hur, and Wadi Lezel, 3 - Wadi Arrajd, 4 - Wadi Eskaikima.

Figure 3b shows much reduced values relative to the analogous plot for i1 and i2 (Figure 3a), but the pronounced maximum in the northeastern parts of the domain still stands out from the background. The linear regression between the two interferograms is very close to the diagonal with a gradient of 0.95 (Figure 4b), suggesting that the scatter is mainly the result of noise and effects of the viewing geometry.

TRMM estimates indicate very little precipitation during the 35-day period covered by interferogram i3 (20041102-20041207) with a spatially averaged accumulation of only 2 mm (9 mm maximum) (Figure 5b). This seems insufficient to generate any significant fluvial sediment movements, so that the signals found in Figure 3b are most likely due to viewing geometry despite the small differences in base lines

Table 1. Interferometric Pairs With a Perpendicular Baseline Difference Less Than 600 m (Track 409) for 2003–2010^a

	Date 1	Date 2	⊥ Baseline Difference (m)	Total Rainfall (mm)	m	b	y(1)
i1	2003-12-23	2004-01-27	256	0	–	–	–
i2	2004-08-24	2004-09-28	284	15	0.60	0.21	0.81
i3	2004-11-02	2004-12-07	286	2	0.85	0.03	0.98
i4	2010-04-20	2010-05-25	310	0	0.79	0.18	0.97
i5	2010-08-03	2010-09-07	157	21	0.68	0.18	0.86

^aFirst pair i1 is used as reference here. Total rainfall amount is taken from TRMM 3B42 estimates over the domain 27.25–28.25°N 10.75–9.5°W. Correlation coefficient γ represents the mean level of correlation for the area between 27.4°N and 28.2°N. Parameters for the linear best fit equation ($y(x) = m \cdot x + b$) defining slope and intercept are given by m and b , respectively; $y(1)$ gives the intercept of the regression line with $x = 1$.

between the two pairs (Table 1). Aeolian erosion may contribute significantly to decorrelation observed over the alluvial fan regions downstream Wadi Lezel and Wadi S’hur.

[29] Interferogram i4 (20100420-20100525; Figure 2d) shows the highest level of coherence with a spatial average of 0.69 despite the fact that this pair has the largest baseline difference (Table 1). Looking at the ratio between i1 and i4 (Figure 3c) reveals some similarities to Figure 3b in the

northeastern parts of the domain, but also some weaker signal in the area of the wadis Esfeisifa and Afra as well as in the center west of the domain. Some of the conspicuous red areas in the northeast suggest that Aeolian erosion is likely to contribute to the observed decorrelation. This is reflected in the scatterplot by a tendency to populate the top left corner, leading to a flatter regression line with a gradient of 0.79, while the area of high coherence falls close to the

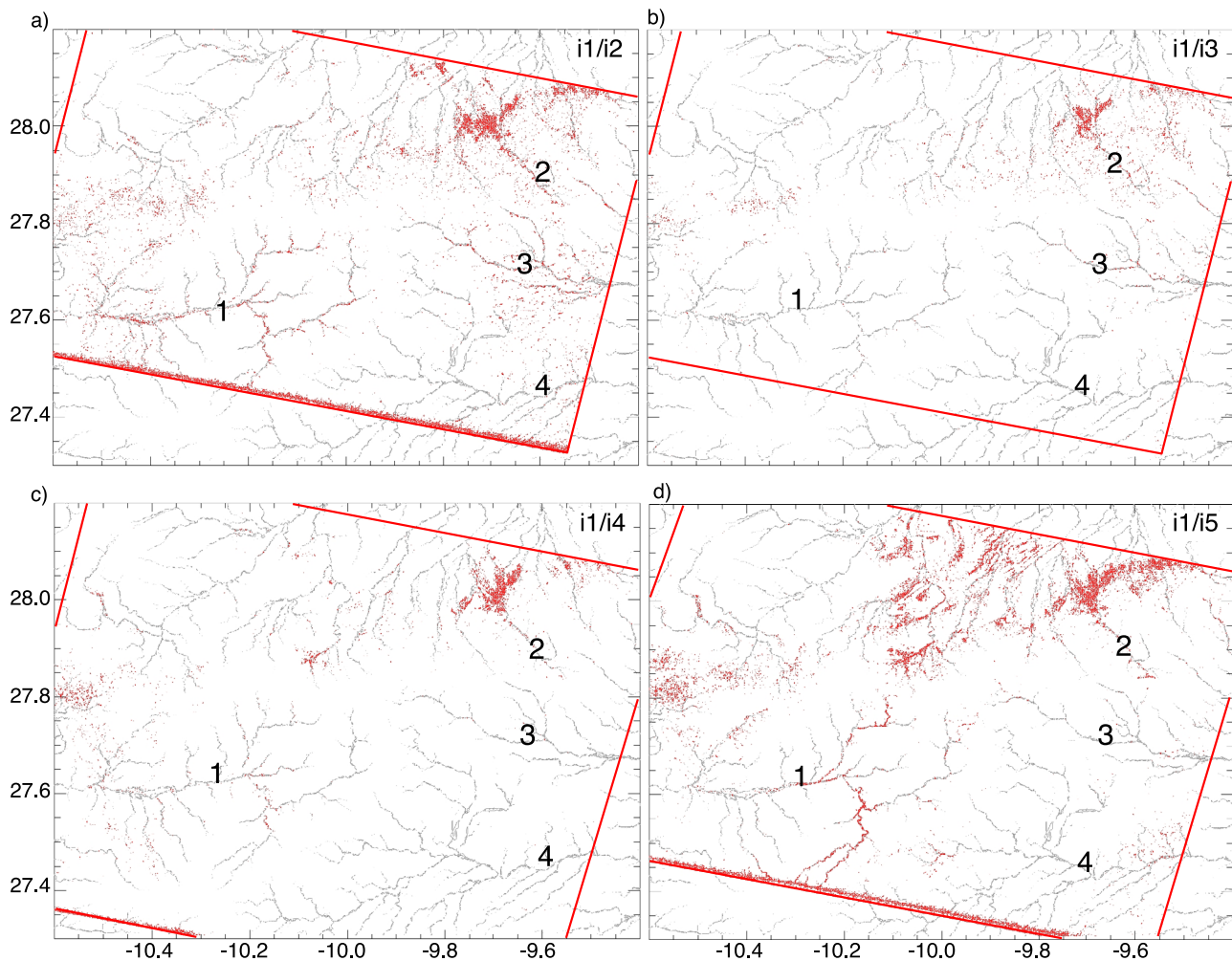


Figure 3. Ratio of coherence for interferograms i2 (a), i3 (b), i4 (c), and i5 (d) against the reference interferogram i1. Areas with values larger than 2 (red) show a significant loss in coherence relative to i1. The location of drainage systems are given in grey where the logarithm of the flow accumulation is larger than 7. Numbers refer to geographical names given in the text: 1 - Wadi Afra, 2 - region of Wadi Umm-Duhl, Wadi S’hur, and Wadi Lezel, 3 - Wadi Arrajd.

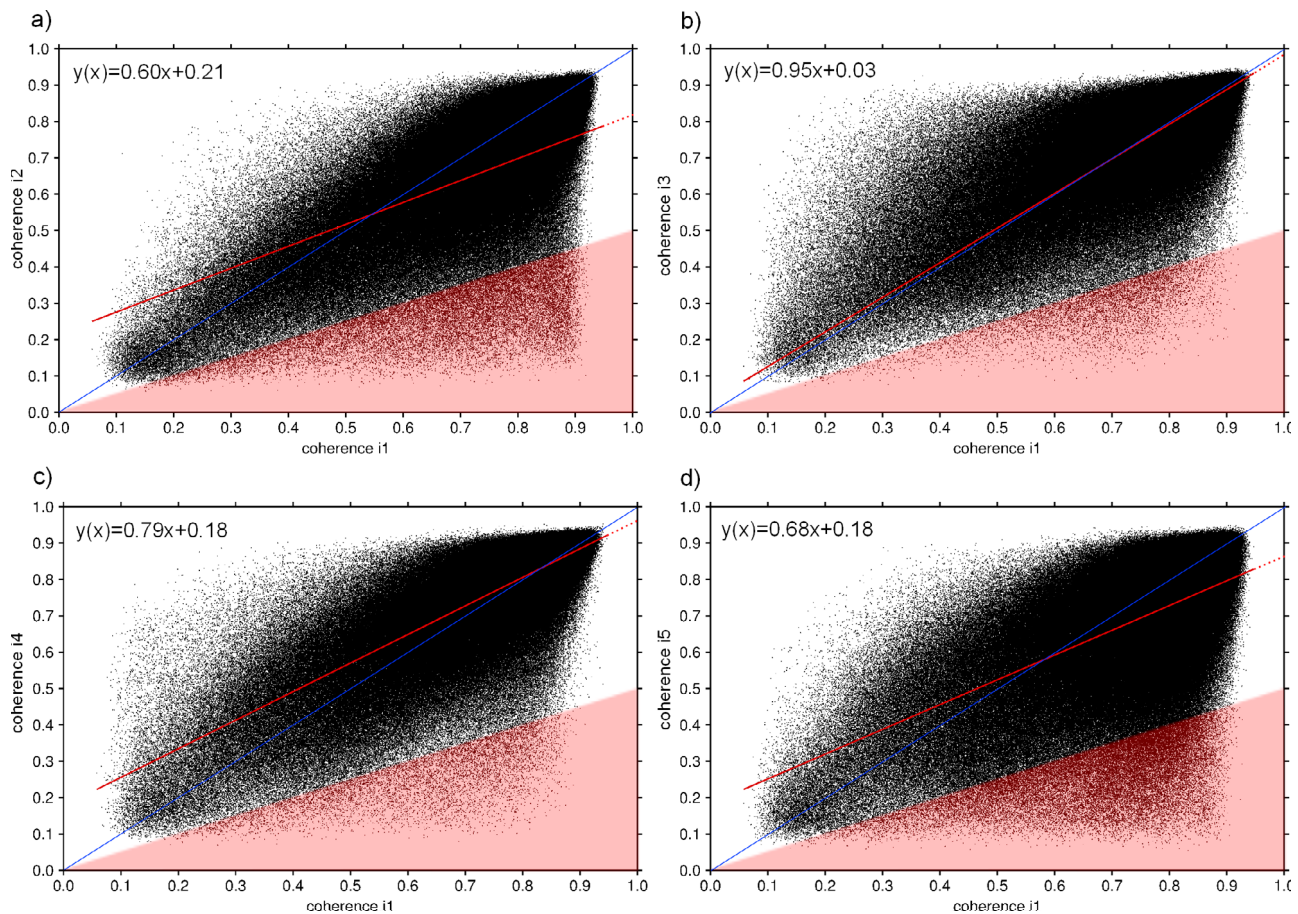


Figure 4. Scatterplots of the interferograms (a) i2, (b) i3, (c) i4, and (d) i5 against the reference interferogram i1. Linear regression fit line is overlaid in red, diagonal is given in blue. The red-shaded bottom triangle marks the range of values where the loss of coherence for i2 (Figure 4a), i3 (Figure 4b), i4 (Figure 4c), and i5 (Figure 4d) is larger than i1, assuming a ratio threshold of 2 for significance.

diagonal (Figure 4c). TRMM estimates do not indicate any precipitation at all for the period covered by i4 suggesting that the signals seen in Figure 3c are very unlikely due to the action of water.

[30] Finally, interferogram i5 (Figure 2e) shows substantial differences compared to i1 (Figure 2a) over large parts of the domain. The ratio calculated from i1 and i5 highlights all wadi catchments to the north and west, with fluvial structures being particularly prominent in the Wadi Afra (Figure 3d). As for i2 the scatterplot shows a clear shift of pixels to the red-shaded bottom right corner and a flat regression line with gradient 0.68 (Figure 4d). Several days with heavy precipitation are observed by TRMM during 20100803-20100907 with an area-average total accumulation of 21 mm, which mainly fell during two periods: 15 mm from 2010-08-14 to 2010-08-17 with 8 mm on 2010-08-15 alone and further 5 mm during 2010-09-03 to 2010-09-06. Interestingly, according to TRMM, most precipitation occurred in the southeastern part of the domain (32 mm), where loss of coherence values do not change dramatically (Figure 5c). This is most likely related to the relatively gently slopes in this area. Nevertheless it appears quite likely that a

significant fraction of the pixels with large decorrelation in other areas in Figure 3d are related to rainfall and runoff.

[31] Pixel-based regression analysis as shown in Figure 4 is a useful way to summarize the complex information provided by spatial maps. However, the gradient of the regression line is less clearly related to precipitation as one might have expected. This is mainly due to the behavior of pixels with low coherence in the reference interferogram, which is not straight-forward to interpret. Therefore it is suggested here to concentrate on the intercept of the regression line with $x = 1$, which is strongly controlled by the decorrelation of pixels with initially high coherence. This parameter is expected to be close to 1 in dry cases such as i3 (0.98) and i4 (0.97), and much lower in wet cases such as i2 (0.81) and i5 (0.86). There are a number of possible explanations why i5 has a higher value than i2 despite the higher area-averaged precipitation: (a) uncertainties in TRMM, (b) concentration of the rainfall on the flatter parts of the domain in the southeast, (c) lower rainfall intensity (as discussed above), (d) a smaller baseline difference (see Table 1), and (e) longer temporal period since the reference interferogram. A deeper analysis of these factors is beyond the scope of this study and

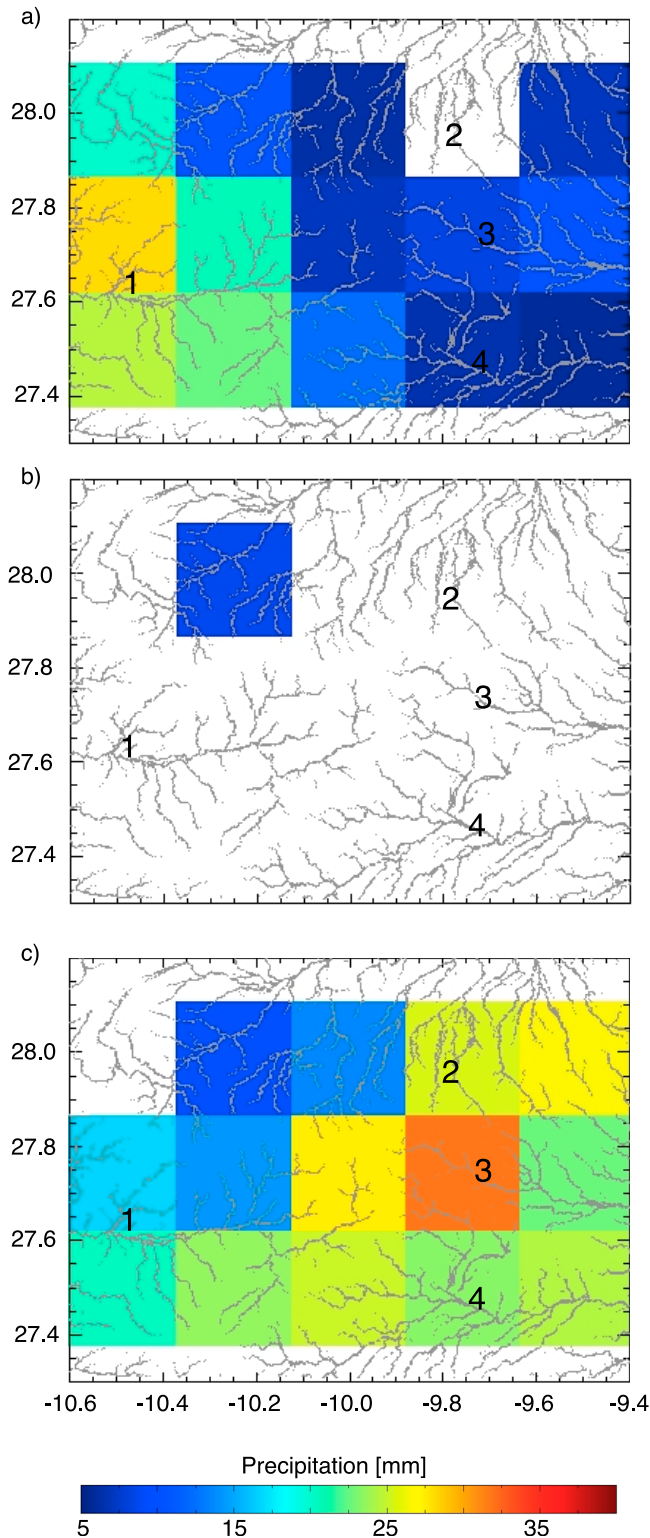


Figure 5. TRMM 3B42 estimated rainfall amounts accumulated for the 35-day periods (a) 20040824–20040928 (i2), (b) 20041102–20041207 (i3), and (c) 20100803–20100907 (i5). Wadis are given in grey. Numbers refer to geographical names given in the text: 1 - Wadi Afra, 2 - region of Wadi Umm-Duhl, Wadi S’hur, and Wadi Lezel, 3 - Wadi Arrajd.

very difficult in case of (a). However, particularly the latter two factors could be analyzed statistically for a much larger data set than investigated here.

5. Discussion and Conclusion

[32] Flash floods are an ubiquitous and important feature in arid areas around the world, but monitoring of these is usually challenging due to their unpredictable nature and inaccessibility of the areas of occurrence.

[33] In this feasibility study, the loss of interferometric phase coherence between two SAR images is analyzed as an indicator for changes in the soil surface in a small test area in northwestern Africa. The InSAR coherence data are combined with satellite-based rainfall estimates and topographic information to aid the assignment of coherence losses to sediment transport due to flash floods. Due to the aridity of the study area the impact of vegetation growth and anthropogenic activity on the coherence can be assumed to be low. Seasonal growth and decay of vegetation may occur and reduce the coherence between two radar images. Vehicle tracks, a likely signature of human activity in arid environments, would be represented by relatively straight, artificial lines in the coherence images. None are identified over the study area. Although we cannot rule out that groups of nomadic people inhabit the study area during the discussed periods, the observed loss of coherence cannot be explained by grazing itself as the vegetation is minimal. Different viewing geometry, however, has a significant impact due to foreshortening and overlay where the terrain is inclined by more than 23° . Aeolian erosion, in particular from the alluvial deposits over the dry floodplains in the northern part, may contribute to decorrelation as well.

[34] Using five interferograms with similar baselines, we show that this method is generally capable of identifying rainfall-induced soil changes, mainly in areas where the surface water runoff accumulates (wadis, drainage systems, desert valleys). Comparisons between a dry and two wet interferograms show a significantly reduced coherence in the latter. We speculated that the detailed relationship between area accumulated precipitation and this coherence loss will depend on the rainfall intensity and spatial distribution relative to steep topography. Comparison between dry interferograms, however, indicates a substantial level of uncertainty, which could be related to viewing geometry, vegetation growth/decay, Aeolian effects on the soil, atmospheric signals such as difference in water vapor and other factors.

[35] In the future, more robust statistics on a larger number of cases is needed to corroborate these results and to reduce uncertainties from effects other than rainfall. Such an analysis will be greatly facilitated once the new InSAR satellite Sentinel-1 will be in orbit (launch date planned for 2013).

[36] In addition, many areas prone to flash floods are also known dust sources with significant contribution to the local dust burden. The combination of InSAR and satellite rainfall estimates presented here is a promising tool to investigate the relation between flash flooding and surface changes as they are relevant for estimating dust emission fluxes due to supply of sediment. The high spatial resolution of the InSAR data will allow a detailed analysis of the location of active dust sources relative in time to the last significant flash flood

event. Such an analysis has the potential to help explain the long-standing issue of the role of soil processes in interannual dust source variability.

[37] **Acknowledgments.** This work is part of the EUFAR (European Facility for Airborne Research) project RAIN4DUST, funded by the European Commission under FP5/FP6/FP7. K.S. and P.K. also acknowledge funding from European Research Council grant 257543 “Desert Storms.” T.J.W. is supported by a Royal Society University Research Fellowship. Access to ENVISAT ASAR images is funded through ESA Category 1 data project 9464. Many thanks go to GES DISC DAAC for compiling and providing TRMM 3B42 rainfall and to MODIS Land team for calculating and providing MYD13Q1.5 NDVI data. Thanks go to Michael Mischuraw for his help translating the geographical names used in this study, and Eric Fielding and two anonymous reviewers whose comments greatly helped to improve the manuscript.

References

- Ahmed, R., P. Siqueira, S. Hensley, B. Chapman, and K. Bergen (2011), A survey of temporal decorrelation from spaceborne L-Band repeat-pass InSAR, *Remote Sens. Environ.*, *115*, 2887–2896, doi:10.1016/j.res.2010.03.017, 2011.
- Bagnold, R. A. (1941), *The Physics of Blown Sand and Desert Dunes*, 265 pp., Methuen, New York.
- Burgmann, R., P. A. Rosen, and E. J. Fielding (2000), Synthetic aperture radar interferometry to measure Earth’s surface topography and its deformation, *Annu. Rev. Earth Planet. Sci.*, *28*, 169–209, doi:10.1146/annurev.earth.28.1.169.
- Chiu, L., Z. Liu, J. Vongsaard, S. Morain, A. Budge, P. Neville, and C. Bales (2006), Comparison of TRMM and water district rain rates over New Mexico, *Adv. Atmos. Sci.*, *23*(1), 1–13.
- Crouvi, O., K. Schepanski, R. Amit, A. R. Gillespie, and Y. Enzel (2012), Multiple dust sources in the Sahara Desert: The importance of sand dunes, *Geophys. Res. Lett.*, *39*, L13401, doi:10.1029/2012GL052145.
- Esteves, M., and J. M. Lapetite (2003), A multi-scale approach of runoff generation in a Sahelian gully catchment: A case study in Niger, *Catena*, *50*, 255–271.
- Fanning, P. C. (1999), Recent landscape history in arid western New South Wales, Australia: A model for regional change, *Geomorphology*, *29*, 191–209.
- Fensholt, R., K. Rasmussen, T. T. Nielsen, and C. Mbow (2009), Evaluation of Earth observation based long term vegetation trends—Intercomparing NDVI time series trend analysis consistency of Sahel from AVHRR GIMMS, Terra MODIS and SPOT VGT data, *Remote Sens. Environ.*, *113*, 1886–1898, doi:10.1016/j.rse.2009.04.004.
- Fielding, E. J., M. Talebian, P. A. Rosen, H. Nazari, J. A. Jackson, M. Ghorashi, and R. Walker (2005), Surface ruptures and building damage of the 2003 Bam, Iran, earthquake mapped by satellite synthetic aperture radar interferometric correlation, *J. Geophys. Res.*, *110*, B03302, doi:10.1029/2004JB003299.
- Friedman, J., W. R. Osterkamp, and W. M. Lewis Jr. (1996), Channel narrowing and vegetation development following a Great Plains flood, *Ecology*, *77*(7), 2167–2181.
- Gillette, D. A., J. Adams, A. Endo, D. Smith, and R. Kihl (1980), Threshold velocities for input of soil particles into the air by desert soils, *J. Geophys. Res.*, *85*, 5621–5630.
- Gillette, D. A., J. Adams, D. Muhs, and R. Kihl (1982), Threshold friction velocities and rupture moduli for crusted desert soils for the input of soil particles into the air, *J. Geophys. Res.*, *87*, 9003–9015.
- Hooper, A., D. Bekaert, K. Spaans, and M. Arikan (2012), Recent advances in SAR interferometry time series analysis for measuring crustal deformation, *Tectonophysics*, *514–517*, 1–13, doi:10.1016/j.tecto.2011.10.013.
- Huffman, G. J., R. F. Adler, D. T. Bolvin, G. Gu, E. J. Nelkin, K. P. Bowman, Y. Hong, E. F. Stocker, and D. B. Wolff (2007), The TRMM Multi-satellite Precipitation Analysis: Quasi-global, multi-year, combined-sensor precipitation estimates at fine scale, *J. Hydrometeorol.*, *8*, 38–55.
- Hughes, A. O., J. M. Olley, J. C. Croke, and L. A. McKergow (2009), Sediment source changes over the last 250 years in a dry-tropical catchment, central Queensland, Australia, *Geomorphology*, *104*, 262–275, doi:10.1016/j.geomorph.2008.09.003.
- Kok, J. F., and N. O. Renno (2009), A comprehensive numerical model of steady state saltation (COMSALT), *J. Geophys. Res.*, *114*, D17204, doi:10.1029/2009JD011702.
- Lee, H., and J. G. Liu (2001), Analysis of topographic decorrelation in SAR interferometry using ratio coherence imagery, *IEEE Trans. Geosci. Remote Sens.*, *39*(2), 223–232.
- Marticorena, B., and G. Bergametti (1995), Modeling the atmospheric dust cycle: 1. Design of a soil-derived dust emission scheme, *J. Geophys. Res.*, *100*(D8), 16,415–16,430.
- Marticorena, B., et al. (2006), Surface and aerodynamic roughness in arid and semiarid areas and their relation to radar backscatter, *J. Geophys. Res.*, *111*, F03017, doi:10.1029/2006JF000462.
- Massonnet, D., and K. L. Feigl (1998), Radar interferometry and its application to changes in the Earth’s surface, *Rev. Geophys.*, *36*(4), 441–500, doi:10.1029/97RG03139.
- Morin, E., T. Grodek, O. Dahan, G. Benito, C. Kulls, Y. Jacoby, G. Van Langhove, M. Seely, and Y. Enzel (2009), Flood routing and alluvial aquifer recharge along the ephemeral arid Kuiseb River, Namibia, *J. Hydrol.*, *368*, 262–275, doi:10.1016/j.hydrol.2009.02.015.
- Okin, G. S. (2007), Relative spectral mixture analysis—A multitemporal index of total vegetation cover, *Remote Sens. Environ.*, *106*, 467–479, doi:10.1016/j.rse.2006.09.018.
- Reheis, M. C., and R. Kihl (1995), Dust deposition in southern Nevada and California, 1984–1989: Relations to climate, source area, and source lithology, *J. Geophys. Res.*, *100*(D5), 8893–8918, doi:10.1029/94JD03245.
- Reynolds, R. L., J. C. Yount, M. Reheis, H. Goldstein, P. Chavez Jr., R. Fulton, J. Whitney, C. Fuller, and R. M. Forester (2007), Dust emission from wet and dry playas in the Mojave Desert, USA, *Earth Surf. Processes Landforms*, *32*, 1811–1827, doi:10.1002/esp.1515, 2007.
- Riley, S. J., S. D. DeGloria, and R. Elliot (1999), A terrain ruggedness index that quantifies topographic heterogeneity, *Intermt. J. Sci.*, *5*(1–4), 23–27.
- Rosen, P. A., S. Henley, G. Peltzer, and M. Simons (2004), Updated repeat orbit interferometry package released, *Eos Trans. AGU*, *85*(5), 47.
- Schaber, G. G., and C. S. Breed (1999), The importance of SAR wavelength in penetrating blow sand in northern Arizona, *Remote Sens. Environ.*, *69*, 87–104.
- Schepanski, K., I. Tegen, B. Laurent, B. Heinold, and A. Macke (2007), A new Saharan dust source activation frequency map derived from MSG-SEVIRI IR-channels, *Geophys. Res. Lett.*, *34*, L18803, doi:10.1029/2007GL030168.
- Schepanski, K., I. Tegen, M. C. Todd, B. Heinold, G. Bönsch, B. Laurent, and A. Macke (2009), Meteorological processes forcing Saharan dust emission inferred from MSG-SEVIRI observations of subdaily source activation and numerical models, *J. Geophys. Res.*, *114*, D10201, doi:10.1029/2008JD010325.
- Schepanski, K., I. Tegen, and A. Macke (2012), Comparison of satellite based observations of Saharan dust source areas, *Remote Sens. Environ.*, *123*, 90–97, doi:10.1016/j.rse.2012.03.019.
- Schmidt, H., and A. Karnieli (2000), Remote sensing of the seasonal variability of vegetation in a semi-arid environment, *J. Arid Environ.*, *45*, 43–59.
- Schwanghart, W., and N. J. Kuhn (2010), TopoToolbox: A set of Matlab functions for topographic analysis, *Environ. Modell. Software*, *25*, 770–781, doi:10.1016/j.envsoft.2009.12.002.
- Shao, Y. (2001), A model for mineral dust emission, *J. Geophys. Res.*, *106*(D17), 20,239–20,254.
- Shao, Y. (2008), *Physics and Modelling of Wind Erosion*, 2nd ed., 452 pp., Springer, New York.
- Smith, L. C. (2002), Emerging applications of Interferometric Synthetic Aperture Radar (InSAR) in geomorphology and hydrology, *Ann. Assoc. Am. Geogr.*, *92*(3), 385–398.
- Weiss, J. L., D. S. Gutzler, J. E. Allred Coonrod, and C. N. Dahm (2004), Long-term vegetation monitoring with NDVI in a diverse semi-arid setting, central New Mexico, USA, *J. Arid Environ.*, *58*, 249–272.